J. Fluid Mech. (1985), *vol.* 159, *pp.* 459–476
Printed in Great Britain

The effects of a strongly temperature-dependent viscosity on Stokes's drag law: experiments and theory

By A. ANSARI AND S. MORRIS
Department of Mechanical Engineering, University of California, Berkeley, CA 94720

(Received 9 August 1983 and in revised form 1 May 1985)

This is an experimental and theoretical study of the slow translation of a hot sphere through a fluid at rest at infinity. The viscosity depends strongly on temperature, i.e., if $\Delta T = T_0 - T_\infty$ is the applied temperature difference and $\gamma = |(\mathrm{d}/\mathrm{d}T_0)\ln\mu(T_0)|$, then the parameter $\theta = \gamma\,\Delta T$ is large: it is about 6.5 in the experiments and is taken as infinite in the theory. The flow is determined by two large parameters, namely the Nusselt number N and the modified viscosity ratio $\epsilon^{-1} = \nu_\infty/(\nu_0\theta^3)$. The qualitative state of the flow is observed to depend on the relation between N and ϵ. If $\epsilon^{-1}\to\infty$ (N fixed, possibly large) previous analysis (Morris 1982) shows that all the shear occurs in a thin low-viscosity film coating the sphere; this film and the associated thermal layer separate at the equator, and a separation bubble of low-viscosity fluid trails the sphere. (ii) If $N\to\infty$ (ϵ^{-1} large but fixed) even the most viscous fluid deforms, and both the drag and heat losses are found to be controlled by this highly viscous flow. The present work maps the major asymptotic states which separate these two end-states for small ϵ. The drag and heat-transfer laws are determined experimentally and theoretically: in addition it is shown that separation of the thermal layer ceases when the drag is controlled by the most viscous fluid, even though the heat transfer in this case can be still controlled by the dynamics of the least-viscous fluid. The heat-transfer and drag laws are also given for a sphere moving in a spherical container of finite radius. This model is shown to give a close estimate of wall effects for a sphere moving in a cylindrical container. For state (i) the theory predicts the heat transfer to within 20% and, for the smallest ϵ, the drag to within 30%. In the experiments ϵ is small enough for all limiting states to be evident but, apart from state (i), a design flaw prevents a quantitative test of the theory. For the other states, the theory is compared with numerical results from Daly & Raefsky (1985). Although the values of ϵ in the calculations are not small enough for the limiting states to be achieved, the theory predicts the drag to within 8% and the heat transfer to within 10%.

1. Introduction

Many creeping flows are greatly influenced by viscosity variations. In compression moulding a polymer charge is squeezed between two parallel disks. The charge is initially cold and is heated by maintaining the two plane faces of the mould at a fixed temperature. This lowers the viscosity near the faces of the mould relative to that in the centre of the charge, and it is observed that in some cases all the shear occurs in the softest fluid, but in others the shear is evenly distributed across the sample (see e.g. Lee *et al.* 1982). If the polymer contains fibres, the differing flow patterns can result in very different mechanical properties in the moulding.

Very similar behaviour occurs in slow flow past a hot sphere (Morris 1982). Fluid ahead of the sphere must deform to pass it. As in compression moulding a continuum of flows is possible: at one extreme all the shear occurs in a thin low-viscosity film coating the forward hemisphere; at the other extreme the isoviscous surroundings of the sphere are deformed over distances comparable to the diameter. Both the heat transfer and drag depend strongly on which type of flow occurs.

Morris (1982) gives the theory covering both the squeezing flow and the flow past a sphere. The theory is stated for the case $\nu(T) = A\,\mathrm{e}^{-\gamma T}$ and assumes that the Reynolds number is zero and that $\theta = \gamma\,\Delta T \to \infty$, where ΔT is the applied temperature difference. The theory for the squeezing flow covers the entire range of behaviour, but that for the sphere assumes that the only shear occurs in the low-viscosity film.

The present work extends the theory for the sphere to cover the remaining limiting states, and then tests the theory experimentally. The experiments provide a quantitative test of the theory for the case in which the only shear occurs in the low-viscosity film but, because of the experimental design, the experiments only demonstrate qualitatively the other limiting states, and the transition to them. The theory for these other limiting states is tested against finite-element calculations by Daly & Raefsky (1985). The main quantitative conclusion from the experiments is that, although the theory assumes $\theta \to \infty$, it predicts the experimental results (for which $\theta \simeq 6.5$) for the heat transfer to within 20 % and for the drag to within 30 %.

The experiments were planned and carried out before the present extension of the theory. In particular when the experiments were designed there was no quantitative theory for the motion of a sphere in the presence of rigid walls, and so the experiment was designed to be quantitative only for the case in which the shear is confined to the low-viscosity layer. In that case the flow is not affected by the presence of the rigid boundaries containing the fluid sample. The resulting data for heat transfer appear to show a systematic offset when deformation of the isoviscous fluid becomes important. This qualitative observation suggested the following rigorous theory which, had it been available when the design was made, would have motivated experiments which gave a quantitative test of the theory even when the isoviscous fluid deforms.

2. Summary of the theory

In this work the sphere is rigid and translates with velocity U through fluid at rest at ∞. The boundary-value problem is

$$0 = \frac{\partial}{\partial x_j}\sigma_{ij} \quad \text{with} \quad \sigma_{ij} = -p\delta_{ij} + 2\mu(T)\,e_{ij}, \tag{1a}$$

$$u_j \frac{\partial T}{\partial x_j} = \kappa \nabla^2 T, \quad \nabla \cdot \boldsymbol{u} = 0. \tag{1b}$$

The boundary conditions are

$$\boldsymbol{u} = \boldsymbol{U}, \quad T = T_0 \quad \text{on } r = a; \quad \boldsymbol{u} \to 0, \quad T \to T_\infty = T_0 - \Delta T \quad \text{as } r \to \infty. \tag{1c}$$

Let D' be the dimensional drag on the sphere; let $P = Ua/\kappa$ and let

$$N = \frac{Q}{2\pi a k\,\Delta T}. \tag{2}$$

Here k is the thermal conductivity of the fluid, a is the radius of the sphere and Q is the total heat flow out of it.

The first difficulty in describing these flows experimentally is the choice of independent variables. Although dimensional reasoning is not particularly helpful, asymptotic analysis makes the choice clear.

It shows that, if $\theta = \gamma \Delta T \to \infty$, the drag and heat-transfer laws take the form

$$P = f(d, \epsilon), \quad N = h(D, \epsilon), \tag{3a}$$

where

$$D = \frac{D'}{\frac{2}{3}\pi\mu_0 \kappa \theta^3}, \quad \epsilon = \theta^3 \frac{\nu_0}{\nu_\infty}. \tag{3b}$$

The choice of D rather than $\epsilon D = D'/\frac{2}{3}\pi\mu_\infty \kappa$ as the first variable is a matter of convenience. Development of the theory was originally motivated by geological applications in which all the shear occurs in the low-viscosity layer (e.g. Morris 1982). In that case the fluid of viscosity μ_∞ does not deform and the drag law does not involve μ_∞: both P and N are then independent of ϵ if D is chosen rather than ϵD. This is particularly useful to note in the experiments. To give a clear demonstration of the limiting states discussed in the introduction, a very large viscosity ratio is needed. In the experiments this is obtained by keeping the ambient fluid at 0 °C and at this temperature μ_∞ is of order 10^8 poise. Viscosities this large are difficult to measure accurately, and the set $\{D, \epsilon\}$ has the advantage that it is easy to fix ϵ by fixing T_0 and T_∞ even if it is difficult to measure it precisely: this allows us to map P as a function of D with ϵ fixed and thus to demonstrate the existence of the two flow states.

The choice of the modified viscosity ratio $\epsilon = \theta^3 \nu_0/\nu_\infty$ is important. Although the theory is stated initially for the viscosity profile $\nu = A\, \mathrm{e}^{-\gamma T}$, Morris (1982, (3.26)) shows that it can be applied to more realistic profiles (such as $\nu = A \exp c/T$) provided they can be approximated by the form $\nu = A\, \mathrm{e}^{-\gamma T}$ for temperatures close to T_0. This is done by taking

$$\gamma = \frac{\mathrm{d}}{\mathrm{d}T_0} \ln \nu(T_0). \tag{4}$$

It is therefore significant that, according to (3a), N and P depend only on D and ϵ: this means that all viscosity profiles with the same values of θ, μ_0 and ϵ result in the same drag and heat transfer, i.e. the drag and heat transfer are independent of the details of the viscosity profile. Asymptotic analysis shows that this is the case because the fluid deforms appreciably in only two regions: coating the sphere there is a layer of characteristic thickness δ/θ in which the viscosity is of order μ_0; and outside the thermal boundary layer the fluid has uniform viscosity μ_∞. The rapid increase in viscosity away from the hot surface is significant in defining the low-viscosity film, but the detailed variations in μ outside this film are shown to play no role whatever. All viscosity profiles with the same θ, μ_0 and ϵ thus result in the same drag and heat transfer.

Theoretical predictions for $\theta \to \infty$

Morris (1982) shows that for the squeezing flow a single solution is possible which, for sufficiently small ϵ, shows the distinct asymptotic states described in the introduction. In contrast, for the sphere it is not possible to make a single analytic solution covering the continuum of flows, but a separate analytic solution is possible for each of the states. Table 1 summarizes the resulting heat-transfer and drag laws.

	Drag D'	$N(D)$	$N(P)$
$0 \leqslant D \ll 1$ conduction limit	$\frac{2}{3}\pi\mu_0 Ua\theta^3$	2	2
$1 \ll D \ll \epsilon^{-\frac{4}{3}}$ lubrication limit	$\frac{1}{24}\pi\mu_0(a^4U^4/\kappa^3)\theta^3$	$D^{\frac{1}{3}}$	$\frac{1}{2}P$
$\epsilon^{-\frac{4}{3}} \ll D \ll \epsilon^{-2}$ intermediate limit	$\frac{4}{3}\pi\mu_\infty aUK(\lambda)$	$1.542D^{\frac{1}{3}}$	$1.834(P/\epsilon)^{\frac{1}{3}}K^{\frac{1}{3}}(\lambda)$
$\epsilon^{-2} \ll D \ll t^4\epsilon^{-3}$ Stokes limit	$\frac{4}{3}\pi\mu_\infty aUK(\lambda)$	$0.650(\epsilon D/K(\lambda))^{\frac{1}{2}}$	$0.922P^{\frac{1}{2}}$

TABLE 1. Asymptotic forms for a solid sphere. $K(\lambda)$ is the correction factor for wall effects, and is given by (6); $\lambda = a/R$ is the ratio of sphere radius to container radius. For an infinite fluid $(\lambda \to 0)$ $K(\lambda) \to 1$. $N = Q/2\pi ka\,\Delta T$.

The entries in the first two rows follow from the theory in Morris (1982, §4). The relation between N and P in the fourth row is simply that for isoviscous flow past a traction-free sphere: that relation (with a slightly different definition of N) is given by Levich (1962, p. 404). The drag law in the fourth row, together with all the entries in row 3, are given by a new analysis in §3. Note that, since the experiments are carried out in a finite container, a correction for wall effects is necessary when deformation in the exterior isoviscous fluid is important.

There are three main points of interest in the table. First, for $D \ll \epsilon^{-\frac{4}{3}}$, the theory predicts the drag to be proportional to μ_0 and independent of μ_∞. Secondly, for $D \gg \epsilon^{-\frac{4}{3}}$ it shows that $D' \propto \mu_\infty U$: the drag depends linearly on U and is independent of μ_0. Thirdly, over a wide range of D, $N \propto D^{\frac{1}{3}}$: however comparison of rows 2 and 3 shows that the constant of proportionality increases by about 50% when the stiff fluid deforms appreciably. Morris (1982) found no equivalent offset for the squeezing flow. This is because of an essential geometric difference between the two flows: in the squeezing flow the thermal layer never separates but it does in the flow past a sphere. If the pressure drop across the sphere is too small to make the stiffest fluid deform, as in (*a*) on figure 1, the thermal layer separates at the equator of the sphere: this is shown by Morris (1982, §4). In contrast, the extended theory shows that, if the pressure drop is large enough to deform the stiff fluid, the thermal layer only separates at the rear stagnation point, as shown at (*b*) in figure 1. The motion of the separation point towards the back of the sphere increases the effective area across which heat is lost. Thus when the pressure field (and hence the drag) is controlled by the exterior flow, the heat transfer is also increased. We shall see that, although the slope of the (N, D)-curve does not change at this transition, the increase in effective area causes an offset in the curve.

3. Flow past a hot sphere for $\epsilon^{-\frac{4}{3}} \ll D \ll \epsilon^{-2}$

This section gives a self-consistent theory for this asymptotic state for a sphere of radius a in a spherical container of radius R. The inner sphere is in pure translation and at the instant of observation is concentric with the outer sphere. This formulation is useful because (as we shall see) it allows direct comparison with numerical studies by Daly & Raefsky (1985). The gap width $R-a$ is assumed large compared to the thermal boundary-layer thickness δ.

In addition to the general assumption $\theta \to \infty$, four assumptions are made here which

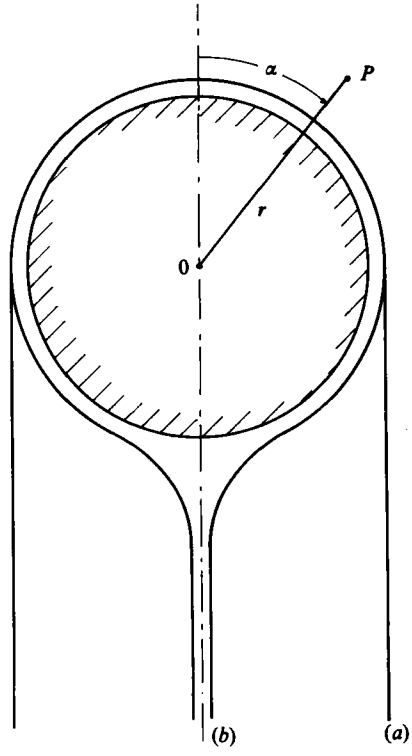

FIGURE 1. Sketch showing (*a*) the isotherms separating at the equator when the pressure drop across the sphere is too small to deform the external isoviscous fluid (lubrication limit, $D \ll \epsilon^{-\frac{4}{3}}$) and (*b*) the isotherms separating only at the trailing stagnation point when the pressure drop is large enough to deform the exterior fluid ($\epsilon^{-\frac{4}{3}} \ll D$).

are specific to the asymptotic state being investigated. These are: (i) the soft layer carries a negligible fraction of the total volume flux past the sphere (so that the exterior flow sees the surface $r = a$ as impermeable); (ii) the exterior flow sees the surface $r = a$ as traction-free; (iii) the soft layer carries essentially all the volume flux along the thermal layer; and (iv) the thermal layer separates only at the rear stagnation point. Note that assumptions (i) and (iii) can be compatible for this state because $\delta \ll a$. Note also that from assumption (ii) the exterior isoviscous flow is completely independent of the boundary condition actually applied to the tangential velocity at $r = a$: that boundary condition only affects the flow in the soft layer. The results of the analysis will be shown to be consistent with these assumptions if $\epsilon^{-\frac{4}{3}} \ll D \ll \epsilon^{-2}$. The first three assumptions can be motivated using the scaling analysis in Morris (1982).

3.1. *Asymptotic analysis*

3.1.1. *The isoviscous exterior*

From assumptions (i), (ii) and (iv) above it follows that the isoviscous flow is simply that due to the translation of an impermeable, traction-free sphere within a spherical container. Happel & Brenner (1965, pp. 120, 131) give the solution. In particular the pressure on $r = a$ is

$$p = \rho \nu_\infty K(\lambda) \frac{U}{a} \cos\alpha, \tag{5}$$

where (r, α, ϕ) are the usual spherical polar coordinates (figure 1), $\lambda = a/R$ and

$$K(\lambda) = \frac{1+5\lambda^3+\frac{5}{2}\lambda^5}{1-\frac{9}{2}\lambda+\frac{9}{2}\lambda^5-\lambda^6}. \tag{6}$$

(The wall correction $K(\lambda)$ in (6) is not the wall correction denoted by the same symbol in Happel & Brenner.) We now show that, because the soft layer is thin, the tangential pressure gradient does not change across it. This externally imposed pressure gradient drives a flow in the soft layer and, since the tangential velocity increases with α, the layer entrains fluid. This entrainment velocity maintains the thermal layer, and hence controls the heat loss.

3.1.2. *The soft layer*

Let $(u_r, u_\alpha, u_\phi) = (w, u, 0)$. Let a circumflex denote dimensionless quantities that are $O(1)$ within the soft layer, and let a tilde denote those that are $O(1)$ over distances of the order of the characteristic thermal-layer thickness δ_0. The following choice of scales can be motivated by scaling (Morris 1982, (2.5)). Here it suffices to note that these scales result in governing equations all with coefficients $O(1)$ in the asymptotic regime of interest. Let

$$r = a+\delta_0\tilde{r} = a+l_0\hat{r}, \quad u = \frac{a}{l_0}w_0\hat{u}, \quad w = w_0\hat{w}; \tag{7a}$$

$$\nu = \nu_0\hat{\nu}, \quad \frac{T-T_\infty}{\Delta T} = \tilde{T} = 1-\frac{1}{\theta}\hat{T}, \quad p = \rho\nu_\infty\frac{U}{a}\hat{p}. \tag{7b}$$

Further, let

$$\epsilon = \frac{\theta^3\nu_0}{\nu_\infty}, \quad w_0 = \frac{U}{\Delta}, \quad \delta_0 = \frac{\kappa}{w_0}; \tag{7c}$$

where

$$\delta_0 = \theta l_0, \quad \Delta = \left(\frac{a}{l_0}\right)^3\frac{\nu_0}{\nu_\infty} = (\epsilon P^3)^{\frac{1}{4}}. \tag{7d}$$

From now on we delete the circumflexes from dimensionless quantities but shall retain the tildes. On letting $l_0/a \to 0$ with P fixed the dimensionless governing equations become

$$\frac{\partial w}{\partial r}+\frac{1}{\sin\alpha}\frac{\partial}{\partial\alpha}(u\sin\alpha) = 0, \tag{8a}$$

$$\frac{\partial p}{\partial r} = 0, \quad \frac{\partial p}{\partial\alpha} = \frac{\partial}{\partial r}\left(\nu\frac{\partial u}{\partial r}\right), \tag{8b, c}$$

$$\nu = e^T, \quad \frac{\partial^2 T}{\partial r^2} = 0. \tag{8d, e}$$

The dimensionless equations (8) are exactly those governing the flow in the lubrication limit $1 \ll D \ll \epsilon^{-\frac{4}{3}}$ (Morris 1982, §4). However the scale for the pressure (7*b*) is different because the driving pressure here is known from (5); in dimensionless variables, it is

$$p = K(\lambda)\cos\alpha. \tag{9}$$

In contrast with the flow in the lubrication limit, here the normal component of velocity is not known at the outer edge of the soft layer, but is to be determined as part of the analysis. The boundary conditions are

$$0 = T = u = w \quad \text{on } r = 0; \quad u \to 0 \quad \text{as } r \to \infty, \tag{10}$$

together with a matching condition on T as $r \to \infty$.

The expressions

$$w = -\frac{1}{\sin\alpha}\frac{\partial\psi}{\partial\alpha}, \quad u = \frac{1}{\sin\alpha}\frac{\partial\psi}{\partial r} \tag{11}$$

exactly satisfy the equation of continuity (8*a*). From the energy equation (8*e*) it follows that

$$T = r/l(\alpha), \tag{12}$$

where the arbitrary function $l(\alpha)$ is fixed by matching (12) to the solution of the external-energy equation. From (12) $\nu = \mathrm{e}^{r/l(\alpha)}$. Let $\zeta = r/l(\alpha)$. The momentum equation (8*c*) then admits a similarity solution of the form

$$\psi = K(\lambda)\, l^3(\alpha)\sin^2\alpha\, f(\zeta). \tag{13}$$

Substitution in (8*c*) shows that the solution $f(\zeta)$ satisfying the boundary conditions (10) is

$$f(\zeta) = 1-(1+\zeta)\,\mathrm{e}^{-\zeta}, \quad f'(\zeta) = \zeta\,\mathrm{e}^{-\zeta}. \tag{14}$$

Let $\mu = \cos\alpha$. Then from (11) and (13) it follows that the entrainment velocity $w(\mu) \equiv w(\infty, \alpha)$ is given by

$$w(\mu) = K(\lambda)\frac{\mathrm{d}}{\mathrm{d}\mu}(1-\mu^2)\, l^3(\mu). \tag{15}$$

Another equation connecting $w(\mu)$ and $l(\mu)$ follows on solving the external-energy equation

$$w(\mu)\frac{\partial\tilde{T}}{\partial\tilde{r}} = \frac{\partial^2\tilde{T}}{\partial\tilde{r}^2}. \tag{16}$$

The solution which matches the solution of the energy equation in the soft layer is

$$\tilde{T} = \exp\tilde{r}\,w(\mu).$$

The arbitrary function $l(\mu)$ in (12) can now be determined by matching. Carrying this out in the usual way, we find

$$w(\mu)\, l(\mu) = -1. \tag{17}$$

Combining (17) with (15) results in the final expression for $l(\mu)$:

$$-1 = K(\lambda)\, l\frac{\mathrm{d}}{\mathrm{d}\mu}(1-\mu^2)\, l^3. \tag{18}$$

This is to be integrated subject to the condition that $l(\mu)$ remains finite at the forward stagnation point ($\mu \to 1$). Let $\lambda = K^{\frac{1}{4}} l(1-\mu^2)^{\frac{1}{3}}$. Then the solution of (18) is given by

$$\lambda^4(\mu) = \frac{4}{3}\int_\mu^1 \mathrm{d}\sigma\,(1-\sigma^2)^{\frac{1}{3}}. \tag{19a}$$

In particular,

$$\lambda^4(-1) = 2.2435. \tag{19b}$$

Figure 2 shows $l(\mu)$ for $K(\lambda) = 1$. It is important to note that $l(\mu)$ remains finite all the way to the back of the sphere. This is essentially different from the behaviour in the lubrication limit: there the pressure drop is too weak to deform the isoviscous fluid and the thermal layer separates at the equator. In the lubrication limit essentially all the heat loss occurs from the forward hemisphere; in the present (intermediate) limit, heat is lost from the entire sphere.

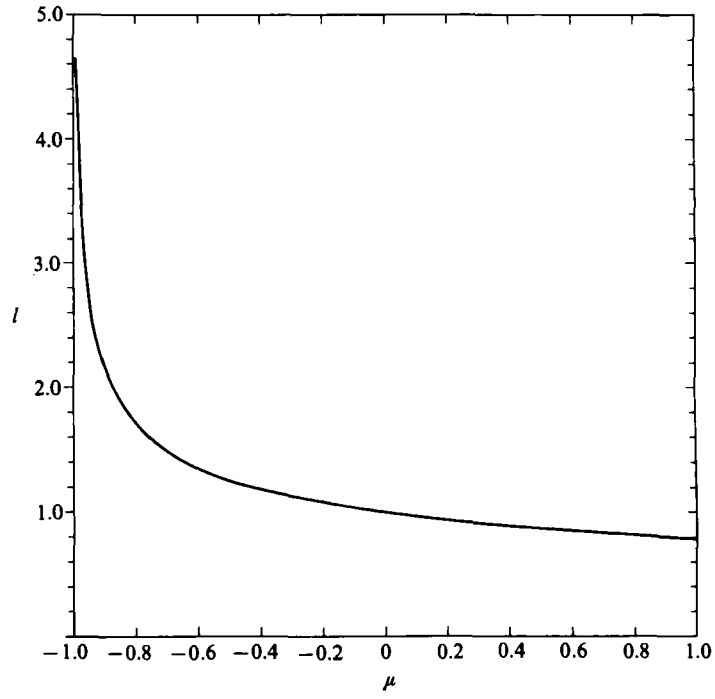

FIGURE 2. Thickness $l(\mu)$ of the soft layer ($l^{-1} = (\partial/\partial\hat{r}) \ln \nu|_{\hat{r}=0}$) when the pressure drop across the sphere is large enough to deform the isoviscous fluid. The layer separates only at the rear stagnation point.

From conservation of energy it follows that the dimensional, thermometric heat flow out of that part of the sphere between $\mu = 1$ and $\mu = \mu_0$ is

$$q(\mu_0) = \int_{S_0} \mathrm{d}S\,(\boldsymbol{u}\cdot\hat{\boldsymbol{n}})\,(T - T_\infty),$$

where S_0 is the conical surface $\mu = \mu_0$, $r \geqslant a$. By assumption (iii), on S_0 $\boldsymbol{u}\cdot\hat{\boldsymbol{n}} = 0$ unless T lies between T_0 and $T_0 - O(\theta^{-1})$ so that T can be replaced by T_0 in the integral. Since $\boldsymbol{u}\cdot\hat{\boldsymbol{n}} = u$, it follows that the dimensionless heat flow is

$$N(\mu) = \frac{q}{2\pi a\kappa\,\Delta T} = \frac{\psi(r=\infty,\mu)}{a\kappa} = \left(\frac{KP}{\epsilon}\right)^{\frac{1}{4}} \lambda^3(\mu). \tag{20}$$

To obtain the last equality we have used (13) and the scales (7c).

The total dimensionless heat flow is

$$N = 1.833\left(K(\lambda)\frac{P}{\epsilon}\right)^{\frac{1}{4}}, \tag{21}$$

if 19(b) is used. Approximately two-thirds of this heat loss is contributed by the forward hemisphere. Since $K(\lambda) \geqslant 1$, the heat transfer is increased by the wall correction. This is the case because a greater pressure drop is needed to force fluid past the sphere when a rigid boundary is present at $r = R$. The increased pressure gradient induces a stronger flow into the soft layer, and this in turn thins the thermal layer and increases the heat flow.

It can now be shown that the normal viscous stresses contribute a drag of order

$(l_0/a)^2$ compared with that due to the pressure. Thus the dimensional drag D' is found by integration of p over the surface of the sphere. This gives

$$D' = \tfrac{4}{3}\pi\rho\nu_\infty a U K(\lambda). \tag{22}$$

In dimensionless form this is $P = \epsilon D/2K$ so that

$$N = 1.541 D^{\frac{1}{4}}. \tag{23}$$

Note that the relationship between N and D is not affected by the presence of the wall at $r = R$.

3.1.3. *Self-consistency*

It remains to show that the results of the theory are consistent with the assumptions on which it is based.

(i) The soft layer carries a negligible fraction of the total volume flux. To show this, note that from (20)

$$\frac{\psi(r=\infty,-1)}{Ua^2} \approx \frac{1}{\epsilon N^3} \approx \frac{1}{\epsilon D^{\frac{3}{4}}}.$$

Hence

$$\frac{\psi(r=\infty,-1)}{Ua^2} \ll 1 \quad \text{if } D \gg \epsilon^{-\frac{4}{3}}. \tag{24}$$

(ii) The exterior flow sees the surface of the sphere as traction-free. To show this note that in the soft layer the shear stress is of order $\mu_0 u_0/l_0$ whereas outside it is of order $\mu_\infty U/a$. From (7), the ratio of these two shear stresses is of order $l_0/a \to 0$, which is the required result.

(iii) The soft layer carries essentially all the volume flux along the thermal layer, and the suction velocity at the outer edge of the soft layer maintains the thermal layer. To show this note that the radial velocity changes between the outer edge of the soft layer and the outer edge of the thermal layer owing to deformation in the external flow. This change is of order $(\delta/a)\,U$, and the ratio of the two contributions to the normal velocity at the outer edge of the thermal layer is of order

$$\frac{a}{\delta_0}\frac{w_0}{U} \approx \frac{1}{\epsilon N^2}, \tag{25}$$

where we have used $N \approx a/\delta_0$ and the definition (7*c*) of w_0. From (23), $N \approx D^{\frac{1}{4}}$ so that, from (25), $aw_0/\delta_0 U \ll 1$ if $D \ll \epsilon^{-2}$. Hence the suction velocity maintains the thermal layer if $D \ll \epsilon^{-2}$. Moreover, the ratio of the volume flux carried by the soft layer to that carried by the isoviscous flow is of order $a^2 w_0/a\delta_0 U$. From (25) this is large if $D \ll \epsilon^{-2}$.

(iv) The thermal boundary layer separates only at the rear stagnation point. Here, self-consistency follows because $l(\mu)$ is finite except at the rear stagnation point (figure 2).

Thus the analysis is self-consistent if $\epsilon^{-\frac{4}{3}} \ll D \ll \epsilon^{-2}$.

3.2. *Comparison with numerical work*

In all the laboratory and numerical studies of this flow, the drag on the sphere has been increased by the presence of walls containing the working fluid: this is the case even in the numerical work of Daly & Raefsky (1985) who modelled the laboratory set-up numerically. The present model assumes that the drag correction factor for

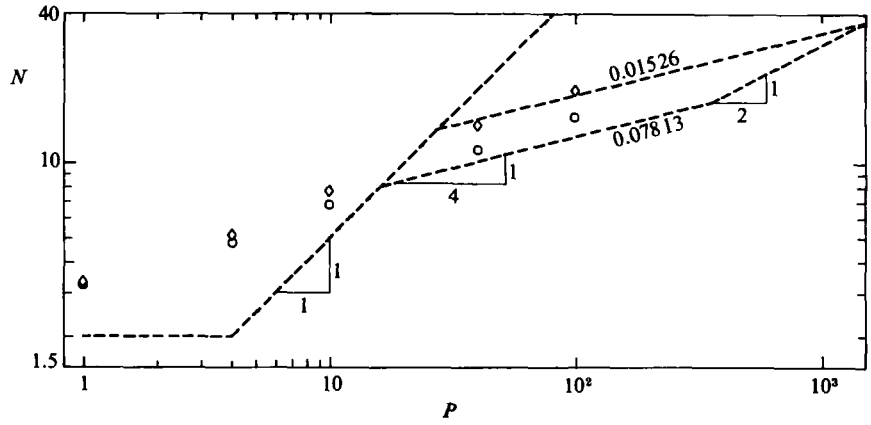

FIGURE 3. Comparison of the asymptotic relations between $N = Q/2\pi a\kappa\Delta T$, $P = Ua/\kappa$ and $\epsilon = \theta^3\nu_0/\nu_\infty$ with results calculated by Daly & Raefsky (1985). The predictions are based on (21) and include wall effects ($\lambda = 0.25$). ○, $\epsilon = 7.81 \times 10^{-2}$: ◇, $\epsilon = 1.53 \times 10^{-2}$.

the hot sphere will not change appreciably if the rigid cylindrical container is replaced by a rigid sphere of the same radius. The point of the model is that, as we have seen, the second case is easily analysed exactly, whereas a treatment of the first is tedious at best.

To justify the assumption, note that for the corresponding isoviscous flow both problems have been solved. For each problem, Happel & Brenner (1965, pp. 133, 320) give $D/6\pi\mu aU$ as a function of $\lambda = a/R$. Comparison of their results shows that if $\lambda \leqslant 0.3$ the two drag corrections agree to within 8%. In the variable-viscosity flow the walls are felt only by the isoviscous exterior flow, and we therefore expect that if the correction factor for a cylindrical container is approximated by that for a spherical container, the error will also be less than 8% for $\lambda \leqslant 0.3$. An error of this magnitude is acceptable in comparing the theory and calculations because, as we shall see, wall effects increase the drag by about 72% in the calculations.

Daly & Raefsky (1985) calculate the flow induced by the axial translation of a hot sphere in a cylinder containing a fluid for which $\nu(T) = A\,\mathrm{e}^{-\gamma T}$. From their equation (34) it follows that $D'/4\pi\mu_\infty aU \to 0.62$ in the intermediate limit $\epsilon^{-\frac{4}{3}} \ll D \ll \epsilon^{-2}$. The limit 0.62 does not depend on whether the inner sphere is rigid or traction free (see their figure 15). This is consistent with our assumption (ii). Moreover, for their calculations $\lambda = 0.25$ and (22) above predicts $D'/4\pi\mu_\infty aU \to 0.574$. The calculated value is 1.08 times the predicted value. The discrepancy is due to the model used above to calculate $K(\lambda)$.

In the calculations of Daly & Raefsky, the smallest $\epsilon = 1.53 \times 10^{-2}$. We shall see later that this is not small enough for the lubrication limit to be apparent in the drag data, and there is little point in comparing theory with calculations for this limit.

Figure 3 shows the asymptotic relations between N and P, including wall effects. The data are from Daly & Raefsky. In the calculations $\epsilon \geqslant 0.015$ and is never small enough for the lubrication limit to be clearly established: however, for the two smallest ϵ, the intermediate limit predicts the heat transfer for $P = 100$ (roughly midway between the two knees) to within 10%. In contrast, in our experiments ϵ was small enough for the intermediate limit to be apparent: the data show that $N \propto P^{\frac{1}{4}}$, but are not accurate enough to establish the constant of proportionality.

Comparison of the theory with the numerical results shows that the theory is predictive in the intermediate limit, but the numerical results are for sufficiently large

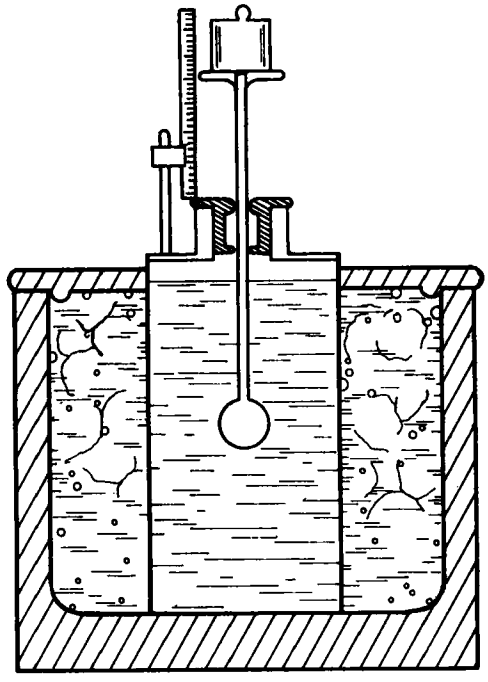

FIGURE 4. The apparatus. The central stainless-steel tank contains the working fluid and is 30 cm high and 20 cm in diameter. The upper surface of the working fluid is free, as discussed in the text. An ice-water bath surrounds the tank and keeps the working fluid at a measured temperature close to 0 °C; this temperature is measured 3 cm off-axis and 7 cm below the fluid surface. The copper ball is forced through the fluid by a weighted plunger passing through a Teflon bearing 5 cm long.

ϵ that the lubrication limit is not clearly visible. In contrast we shall now see that it is relatively easy to test the theory against laboratory experiments in the lubrication limit.

4. Experimental apparatus and procedure

4.1. *Design constraints*

The apparatus was designed to allow a quantitative test of the theory in the lubrication limit together with a qualitative demonstration of the transition to the Stokes limit. Comparison of figures 6 and 7 in Morris (1982) shows that both the (N, D)- and (P, D)-curves will lie on the lubrication asymptote for about 2 orders of magnitude in D if $\epsilon < 2 \times 10^{-3}$. If we assume $\theta = 5$ to be the smallest θ for which the asymptotic theory applies, $\epsilon = 2 \times 10^{-3}$ corresponds to a viscosity ratio ν_∞/ν_0 of order 10^5. To show the transition to the Stokes limit in the drag law for this ϵ the apparatus must be capable of providing a dimensionless buoyancy D of up to 10^4.

4.2. *Apparatus*

The design closely follows that of Ribe (1983) and is shown in figures 4 and 5. There is an air space above the entire free surface of the working fluid. This was originally included because two different sizes of ball were used, and different volumes of fluid were displaced. It has the disadvantage that in the Stokes limit the ball drags down the free surface of the fluid so that the rod and part of the trailing hemisphere are exposed to air. Because of this both the measured heat loss and drag are about half

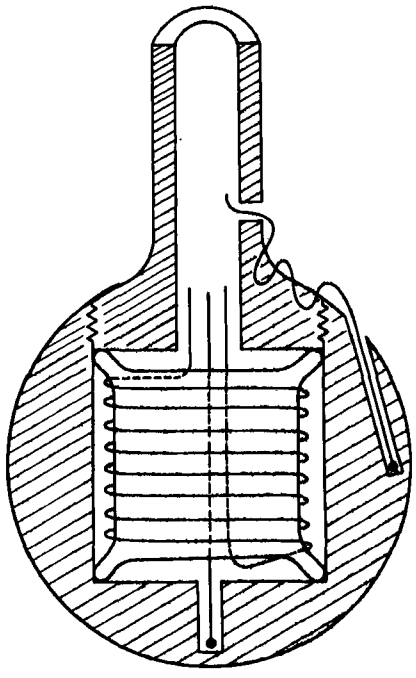

FIGURE 5. The copper sphere. Two different spheres were used: the smaller is 2 cm in diameter with a driving rod 0.4 cm in outside diameter; for the larger the corresponding figures are 4 cm and 1 cm. Each sphere carried 4 thermocouples: the two shown in the figure read the temperature of the copper 0.1 cm below the ball's surface; a third thermocouple is glued to the back surface of the ball and the fourth, to the outside of the rod 2.5 cm behind the sphere. All four readings agree to within 0.5 °C if the leads from the forward thermocouple are insulated from the heater.

the predicted values in the Stokes limit. This does not happen in the lubrication limit. Of course the difficulty could have been avoided by filling the tank flush with its top, and leaving an air space only below the Teflon bearing.

When the apparatus was designed, this did not seem a serious failing. At that stage the behaviour of the separation bubble was unknown and the simple theory for wall effects given in §3 was not possible. This flaw in the design means that the experiments provide only a qualitative test of the theory in the Stokes limit.

4.3. *Working fluid*

This is a viscous corn syrup supplied by CPC International who specify it by a Baume number (45) and a D.E. number (33.5). Table 2 gives its material properties other than the viscosity: these properties were supplied by the manufacturer. The properties at $T = 49$ °C were used to reduce the data.

Figure 6 shows the viscosity as a function of temperature: the three isolated points are measurements taken by Saybolt & Company on a sample we provided; the remaining data were obtained by us using a falling-ball viscometer. The sample analysed by Saybolt & Company contained no air bubbles, but that analysed by us had been used in the experiment and (even after heating) contained many very fine air bubbles. The agreement of the two sets of data for high temperatures suggests that these very small bubbles do not increase μ substantially.

T °C	C_p (J/g °C)	k (W/cm °C)
27	2.21	0.00346
49	2.27	0.00363
71	2.34	0.00377

Density $\rho = 1.44$ g/cm^3
Thermal diffusivity $\kappa = 0.0011$ cm^2/s

TABLE 2. Thermal and physical properties of the corn syrup used in the experiment

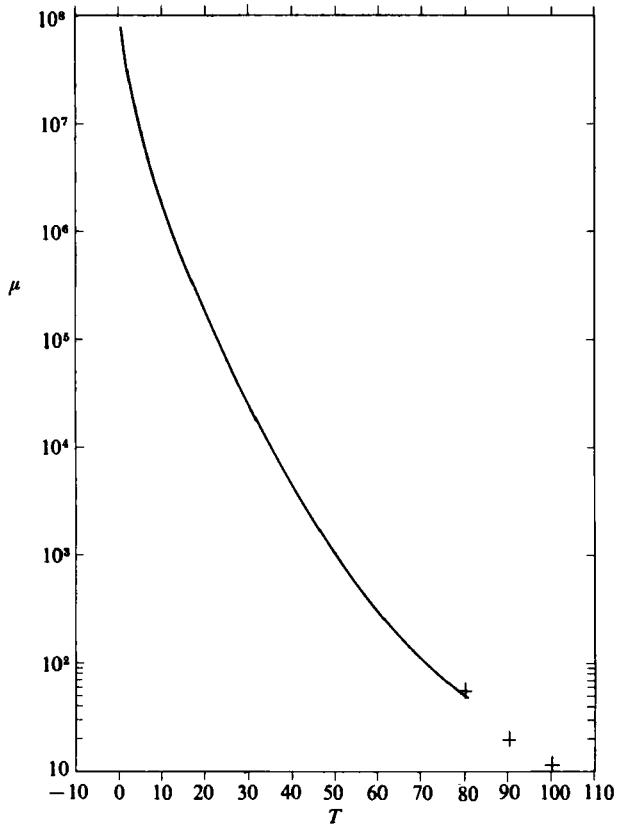

FIGURE 6. Viscosity of the working fluid (poise) as a function of temperature (°C).

4.4. *Experimental procedure*

Each run began by allowing the syrup to come to thermal equilibrium with the ice-water bath. The sphere was suspended just above the fluid and its temperature raised to a given temperature T_0. A specified weight was added to the platform shown in figure 4, and the ball allowed to sink through the fluid. The temperature T_0 was kept constant manually. When the ball was 5–8 cm into the fluid, we recorded the depth of penetration (at 1 cm intervals), the time, T_0, the power supplied to the heater and the load D'. The Nusselt number N is defined by (2) and dimensionless load D, by (3*b*).

There were 63 runs: ϵ was fixed for groups of 10–20 runs and D was varied (by changing the load) to map the drag and heat-transfer curves. The load varied from

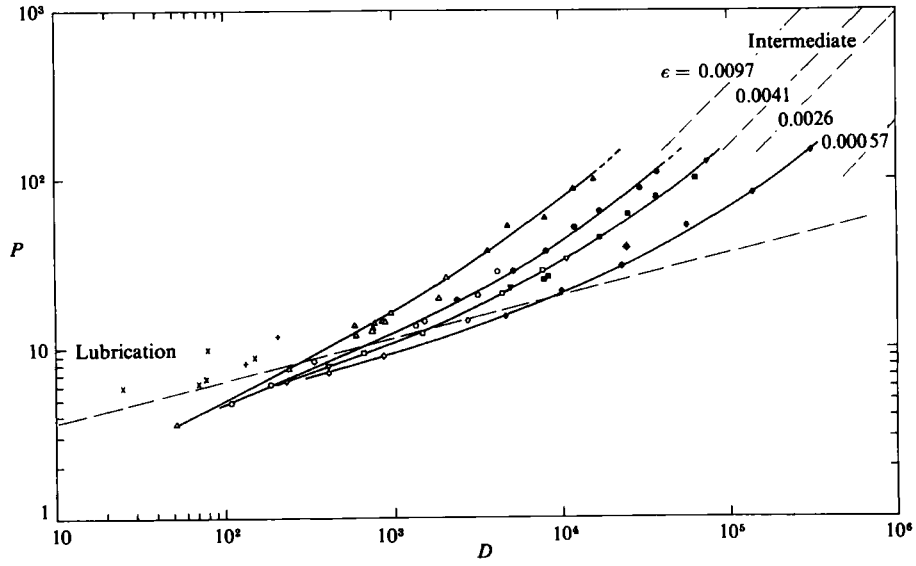

FIGURE 7. Experimental results for $P = Ua/\kappa$ as a function of $D = D'/\frac{2}{3}\pi\mu_0\kappa\theta^3$ and $\epsilon = \theta^3\nu_0/\nu_\infty$. D' is the dimensional drag. Each broken line is the predicted asymptote for the ϵ-value of the right-most point on the corresponding empirical curve: wall corrections are included ($\lambda = 0.2$). The solid curves were fitted by eye to the data before the broken lines were drawn. Open (solid) symbols show data collected for the small (large) sphere. $\times$, $2.1\times10^{-1} \geqslant \epsilon \geqslant 1.1\times10^{-1}$; +, $3.5\times10^{-2} \geqslant \epsilon \geqslant 3.3\times10^{-2}$; $\triangle$, $1.5\times10^{-2} \geqslant \epsilon \geqslant 8.1\times10^{-3}$; $\bigcirc$, $5.3\times10^{-3} \geqslant \epsilon \geqslant 3.4\times10^{3}$; $\triangledown$ & $\square$, $2.6\times10^{-3} \geqslant \epsilon \geqslant 1.5\times10^{-3}$; $\diamond$, $5.3\times10^{-4} \geqslant \epsilon \geqslant 4.7\times10^{-4}$.

50 gm to 4 kg on the small ball, and 0.6 kg to 33 kg for the large ball. For almost all runs T_∞ lay between 0 and 1 °C, and T_0 varied by about 1 °C in a given group. Almost all the runs were taken with $T_0 = 43$, 49, 55 or 66 °C. The smaller ball used between 1 and 15 W, which was supplied by a standard d.c. supply; for the larger ball the range was 15–80 W and a.c. was used.

5. Experimental results

The Appendix gives P and N as functions of D and ϵ for all runs.

5.1. *The drag law*

The drag data are shown in figure 7. The experimental curves show the three important qualitative features predicted by the analysis and discussed in §2.1. First, all the curves collapse to a single curve to the left of the figure: thus for sufficiently small D the drag law becomes independent of the background viscosity μ_∞ and the only deformation occurs in the soft layer. Secondly, for given ϵ the slope of the experimental curve appears to approach one for large enough D: in each case the tangent to the right end of the experimental curve has a slope of approximately 0.80 so that for large enough D the drag law appears to become linear in U. Thirdly, for given D, the slope of the drag curve decreases smoothly as $\epsilon \to 0$: for the smallest $\epsilon = 0.00057$, the slope of the curve for $4.4\times10^2 \leqslant D \leqslant 5.0\times10^3$ is approximately 0.31. According to the theory $P \propto D^{\frac{1}{3}}$ in this lubrication limit.

In addition, for the curve with the smallest $\epsilon = 0.00057$ the drag law for the lubrication limit predicts the observation to within 30% for $480 \leqslant D \leqslant 3.5\times10^4$, i.e. for almost two decades in D.

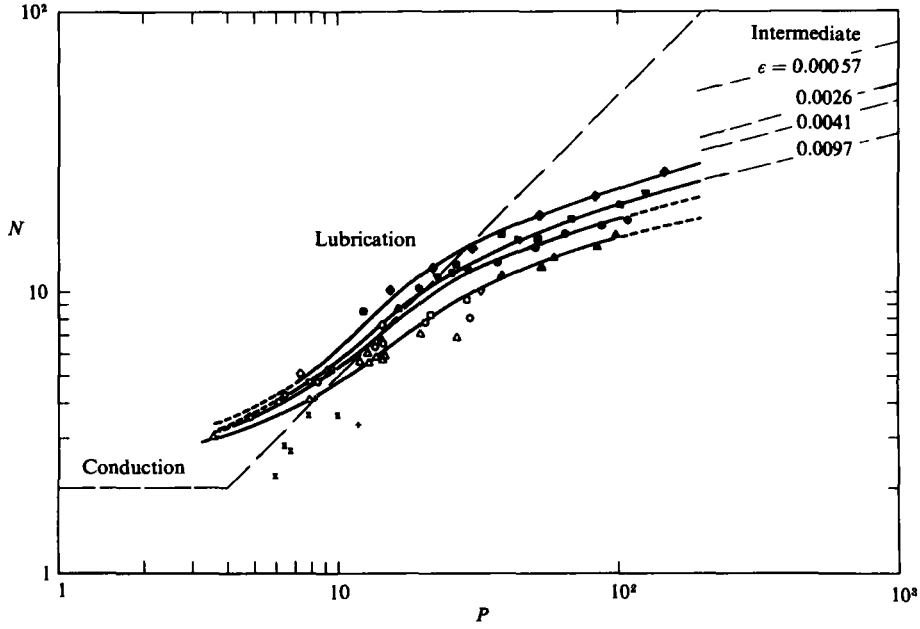

FIGURE 8. Experimental results for $N = Q/2\pi ak\,\Delta T$ as a function of $P = Ua/\kappa$. The broken lines are the predicted asymptotes: their analytic forms are given in table 1 ($\lambda = 0.2$). The solid curves were fitted by eye to the data before the asymptotes were drawn. See figure 7 for symbols.

Even without wall corrections, the predicted drag in the Stokes limit is 1.2–1.6 times the observed drag. Since the discrepancy is systematic, it appears that it is due to the sphere pulling the free surface down, so that the fluid does not completely cover the back hemisphere. We shall see that the data for heat loss supports this idea.

5.2. *Heat losses*

In figure 8 the experimental points are shown by plotting N against P. The theory predicts that for large P, $N \propto P^{\frac{1}{4}}$: the transition to this $\frac{1}{4}$-power law is obvious in the data, but the predicted constant of proportionality is 1.4–2 times the observed constant. Earlier we noted that, in the intermediate limit, the sphere was observed to pull the free surface of the fluid down, so that the back hemisphere was not covered by the fluid in this limit. The reduction in heat loss is a consequence of this; figure 7 shows that the drag is affected in the same way.

Since the displacement of the free surface makes it easier to deform the stiffest fluid, the drag is reduced in the intermediate limit, and the transition from the lubrication to the intermediate limits occurs for smaller P than was predicted. Thus the range of P for which a given curve in figure 8 follows the lubrication curve is reduced. Despite this, the predictions and observations agree to within 20% in the lubrication limit and, in addition, for the smallest ϵ the observed curve has a slope of approximately 0.67 for $7 \leqslant P \leqslant 20$: the theory predicts $N \propto P$.

Figure 9 shows N as a function of D. We consider the results for the small and the large sphere separately. For the small sphere (open symbols) all data for the lubrication limit lie within 20% of the theoretical prediction: however these data continue to lie on the lubrication asymptote even when the theory predicts that the flow should have entered the intermediate limit. This effect is particularly evident when N is plotted against P (figure 8). In that figure these points (open symbols,

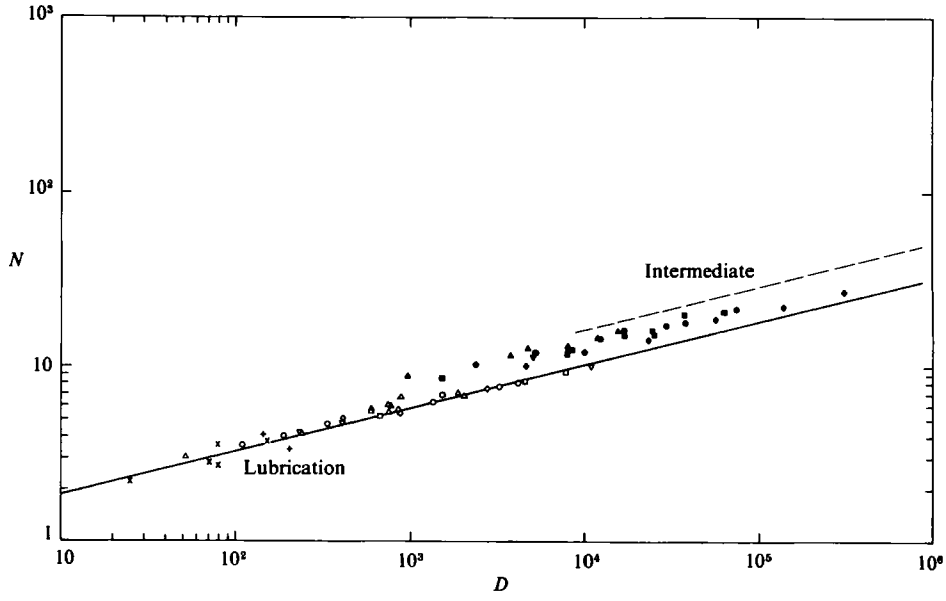

FIGURE 9. Experimental results for Nusselt number $N = Q/2\pi ak\Delta T$ as a function of $D = D'/\frac{2}{3}\pi\mu_0\kappa\theta^3$. The lines with slope $\frac{1}{4}$ are the predicted asymptotes: their analytic forms are given in table 1. See figure 7 for symbols.

$N \geqslant 7$) fall below the empirical curves. Since the empirical (N, P)-curves were determined in the intermediate limit by data taken from the large sphere (figure 8, solid symbols), it appears that there is some dependence on the radius of the sphere. There are two ways in which this could enter. First, conceivably the conduction resistance of the large sphere might be large enough that it becomes a poor approximation to assume a uniform surface temperature for the sphere. However measurements of the surface temperature show that it is uniform to within 0.5 °C: this is small compared with the applied temperature difference which was about 50 °C. Secondly, because the sphere advances in a finite container, there is a return flow. It seems plausible that this return flow will oppose the tendency of the sphere to drag the free surface down: since the return flow is weaker for the smaller sphere ($\lambda = a/R = 0.1$) than it is for the large ($\lambda = 0.2$) it is possible that the back of the small sphere is more exposed to air than is the back of the large sphere. This would explain why the heat loss for the small sphere is reduced relative to that from the large sphere. At present, only the second of these explanations seems possible. We conclude that points marked by open symbols in figure 9, and with $N \geqslant 7$, underestimate the heat loss from the sphere: the error is systematic and appears to be due to the deflection of the free surface.

If N for the large sphere is correlated against D (figure 9, solid symbols), the data lie between the asymptotes for the lubrication and intermediate limits, and there is a systematic dependence on ϵ: those data with the smallest ϵ lie closest to the prediction for the lubrication limit. The systematic dependence on ϵ can be understood by referring to figures 7 and 8: in the intermediate limit both the drag and the heat transfer fall below the predictions, and this happens most strongly for the smallest values of ϵ.

6. Conclusions

The present data show all the qualitative features predicted by the theory. In addition, for the smallest value of ϵ (0.00057) and for $\theta \simeq 6.5$ the theory for the lubrication limit predicts the drag to within 30 % and heat transfer to within 20 %. The experiments are not sufficiently accurate to test the theory in the intermediate limit, but comparison of the theory with numerical experiments by Daly & Raefsky (1985) shows that the theory predicts the heat transfer to within 10 % in the intermediate limit, and the drag to within 8 %. Although the present results are marred by the deflection of the free surface, the essential point is that laboratory experiments are a cheap and effective method of testing asymptotic theories of this type: once the initial design problems have been solved, it is relatively easy to make θ large enough for the asymptotic analysis to apply, and ϵ small enough that the asymptotic states described in the introduction are evident in the results.

This work is supported by the National Science Foundation through grant MEA-8208657 (Morris). The experiments described in §§4 and 5 were carried out by A. Ansari in partial fulfilment of the requirements for the M.Sc. degree in Mechanical Engineering.

Appendix 1. Sorted results, rounded to 3 figures

ϵ	P	N	D
1.27×10^{-1}	6.35	2.80	7.62×10^{1}
1.21	6.75	2.70	8.34
1.14	9.90	3.6	8.44
1.30	7.8	3.7	1.61×10^{2}
1.53×10^{-2}	7.8	4.10	2.54×10^{2}
1.25	13.7	5.8	6.38
1.24	12.9	5.54	7.94
1.04	12.6	6.0	7.99
1.14	14.0	5.86	8.21
1.30	14.4	5.76	9.13
1.09	19.7	7.06	2.00×10^{3}
*1.05	53.0	12.8	5.10
8.7×10^{-3}	3.55	3.02	5.56×10^{1}
9.3	11.9	5.6	6.37×10^{2}
§8.6	14.2	6.72	9.47
*8.9	16.4	8.80	1.03×10^{3}
9.3	26.5	6.8	2.18
*9.0	38.2	11.6	3.91
*8.8	59.7	13.3	8.53
*9.7	85.5	14.6	1.28×10^{4}
*8.1	99.0	16.0	1.69
5.2×10^{-3}	4.80	3.56	1.16×10^{2}
4.8	6.10	4.0	2.02
4.0	8.4	4.74	3.62
5.3	13.7	6.26	1.45×10^{3}
*4.5	19.3	10.2	2.54
4.0	20.3	7.68	3.45

* Large ball. § Cold rod.

Appendix 1 (*continued*)

ϵ	P	N	D
*4.5	51.6	14.5	1.29×10^4
*4.3	64.4	16.2	1.84
*4.1	110	18.0	4.07
3.4×10^{-3}	14.3	6.48	1.63×10^3
3.4	28.6	8.0	4.50
*3.5	28.0	12.1	5.60
*3.7	37.2	12.7	8.67
*3.4	88.1	17.2	3.20×10^4
2.3×10^{-3}	6.40	4.16	2.45×10^2
2.2	7.9	4.72	4.35
*2.3	23.0	11.46	5.46×10^3
2.5	32.7	10.0	1.18×10^4
*2.6	128	21.6	8.05
2.1	9.4	5.24	7.16×10^2
*1.85	12.2	8.48	1.60×10^3
1.5	21.3	8.22	4.84
2.0	29.0	9.28	8.40
$*1.8 \times 10^{-3}$	25.7	11.9	8.50×10^3
*1.57	26.4	12.7	8.98
*1.82	44.3	15.1	1.86×10^4
*1.03	38.7	16.1	2.63
*1.46	52.0	15.3	2.71
*2.0	69.0	19.8	3.98
*1.75	101	20.6	6.89
5.29×10^{-4}	7.2	5.07	4.36×10^2
6.03	9.10	5.35	9.38
6.25	14.3	7.57	2.97×10^3
*4.40	15.3	10.1	5.01
*6.04	21.7	12.1	1.07×10^4
*4.77	30.2	14.3	2.48
*6.67	52.5	18.9	6.08
*5.09	83.0	22.0	1.49×10^5
*5.67	147	26.8	3.30
2.11×10^{-1}	5.88	2.20	2.68×10^2
3.47×10^{-2}	11.9	3.38	2.22×10^3
3.30	8.1	4.12	1.51×10^2

* Large ball.

REFERENCES

Daly, S. F. & Raefsky, A. 1985 On the penetration of a hot diapir through a strongly temperature-dependent viscosity medium. *Geophys. J. R. Astron. Soc.* (In press.)

Happel, J. A. & Brenner, H. 1965 *Low Reynolds-Number Hydrodynamics.* Prentice-Hall.

Lee, S. J., Denn, M. M., Crochet, M. J. & Metzner, A. B. 1982 Compressive flow between parallel disks. *J. Non-Newtonian Fluid Mech.* **10**, 3–30.

Levich, V. 1962 *Physico-Chemical Hydrodynamics.* Prentice-Hall.

Morris, S. 1982 The effects of strongly temperature-dependent viscosity on slow flow past a hot sphere. *J. Fluid Mech.* **124**, 1–26.

Ribe, N. 1983 Diapirism in the Earth's mantle. *J. Volcanol. Geotherm. Res.* **16**, 221–245.